PCCP

ARTICLE TYPE

Cite this: DOI: 00.0000/xxxxxxxxxx

Hydration in aqueous osmolyte solutions: the case of TMAO and urea

Christoph J. Sahle*[a], Martin A. Schroer[b], Johannes Niskanen[c], Mirko Elbers[d], Cy M. Jeffries[b], Christian Sternemann[d]

Received Date
Accepted Date

DOI: 00.0000/xxxxxxxxxx

The hydration and hydrogen-bond topology of small water solvated molecules such as the naturally occurring organic osmolytes trimethylamine N-oxide (TMAO) and urea are under intense investigation. We aim at furthering the understanding of this complex hydration by combining experimental oxygen K-edge excitation spectra with results from spectra calculated via the Bethe-Salpeter equation based on structures obtained from *ab initio* molecular dynamics simulations. Comparison of experimental and calculated spectra allows us to extract detailed information about the immediate surrounding of the solute molecules in the solvated state. We quantify and localize the influence of the solute on the hydrogen bond network of the water solvent and find spectroscopic fingerprints of a clear directional asymmetry around TMAO with strong and local kosmotropic influence around TMAO's NO head group and slight chaotropic influence around the hydrophobic methyl groups. The influence of urea on the local water network is qualitatively similar to that of TMAO but weaker in magnitude. The strongest influence of both molecules on the shape of the oxygen K-edge spectra is found in the first hydration shells.

1 Introduction

Trimethylamine N-oxide (TMAO) is a small organic osmolyte that is found to stabilize proteins in deep sea fish against the high hydrostatic pressures present at great depth[1–3]. Urea, on the contrary, is a strong denaturant at high concentrations and is found as waste product in mammalian kidneys[4]. The molecular mechanisms of these effects have not been completely explained as of yet.

The protein stabilizing effect of TMAO against several perturbations, such as high urea concentrations or high pressure conditions, is well studied and documented[4–9], however, the underlying mechanism is still not entirely understood. Due to its zwitterionic character and its strong dipole moment, TMAO strongly and particularly interacts with the surrounding water molecules, which is assumed to be essential for its stabilization effect[10]. Whereas the direct interaction between chaotropes like urea and the backbone of proteins have been observed[11,12], repulsive interactions between protein stabilizing osmolytes such as TMAO and macromolecules have been reported[4,13,14]. This repulsive force favors hydration of the protein surface possibly rendering the stabilizing effect of TMAO indirect and water mediated[15–18].

More recent simulation studies, however, report on a more direct interaction between TMAO and macromolecules[19–22]. Here, the osmolytes are found to be close to the macromolecules, interacting either directly or via a single layer of water molecules with it. The latter mechanism indeed would result in a preferred hydration[23,24]. These findings are thus questioning an indirect and long-range influence on the water structure on a bulk scale and, therefore, the water-mediated nature of the protein stabilizing mechanism.

Based on a broad range of experimental and simulation studies, it is indeed well established that TMAO strongly affects the water structure[9,10,25–32], which is distinct from the influence of other cosolvents[22,33,34]. The recent findings, however, raise the question about the actual range of this effect on the water structure and its direction dependence with respect to the zwitterionic structure. However, many used experimental probes are not element sensitive, such as X-ray diffraction, or are semi-local, such as IR- and vibrational spectroscopy. As shown recently, the oxygen K-edge excitation spectrum is sensitive to the direct and immediate surrounding of the excited atomic site[33,35–38] and, in particular, in combination with molecular dynamics (MD) simulations and

[a] *European Synchrotron Radiation Facility, 71 Avenue des Martyrs, 38000 Grenoble, France. E-mail: christoph.sahle@esrf.fr*
[b] *European Molecular Biology Laboratory (EMBL), Hamburg Outstation c/o DESY, Notkestrasse 85, Hamburg 22607, Germany*
[c] *Department of Physics and Astronomy, University of Turku, FI-20014 Turun Yliopisto, Finland*
[d] *Fakultät Physik/DELTA, Technische Universität Dortmund, 44221 Dortmund, Germany*

novel quantum mechanical calculations of the site-by-site excitation spectra, insights into the local structure around the excited atom can be extracted[39].

In this study, we explore the microscopic structural details of the hydration of TMAO and its supposed biological adversary urea in aqueous solutions by combining results from atomistic structural simulations based on *ab initio* molecular dynamics (AIMD) and successive oxygen K-edge simulations. This approach allows us to link these statistical simulations with the experimentally accessible oxygen K-edge spectrum of the statistical ensemble average, thus confirming that TMAO strongly binds three water molecules via hydrogen bonding to its NO head group and a chaotropic influence of the hydrophobic methyl groups that affect water molecules in the first hydration shell. Urea shows similar tendencies compared to TMAO but to a lesser degree. Signatures of these atomistic details of the hydration process are clearly extractable from the experimental oxygen K-edge spectra, yielding a unique access to the local structure in the direct vicinity of the studied osmolytes.

2 Methods

2.1 *Ab initio* Molecular dynamics

We performed spectral calculations based on configurations from previously reported AIMD simulations of pure water, water-TMAO solution, and water-urea solution[40–42]. In short, the AIMD run of pure water at ambient conditions consisted of 128 H_2O molecules in a periodic cubic simulation supercell of 15.6627 Å box length. The TMAO-water solution consisted of one TMAO molecule and 107 H_2O molecules in a periodic cubic simulation cell of 14.9382 Å box length. For the urea-water solution, a cubic simulation box of 14.9984 Å box length contained 110 H_2O molecules and one urea molecule. The Born-Oppenheimer AIMD simulations were run using the RPBE functional[43] taking London dispersion interactions into account via Grimme's D3 method[44,45]. All simulations were run for several tens of picoseconds after initial equilibration within the canonical ensemble[40–42].

2.2 Spectrum calculations

Calculations of the non-resonant inelastic X-ray scattering spectra at the oxygen K-edge were performed using the Bethe-Salpeter Equation (BSE) method as implemented in the OCEAN (Obtaining Core level Excitations using Ab initio methods and the NIST BSE solver) code[46,47]. For the calculations, the ground state wave functions and electron densities were computed using density functional theory (DFT) with the Quantum ESPRESSO program package[48,49]. Since we use pseudopotentials for the computation of the ground state electronic properties, projector augmented wave (PAW) reconstructed all-electron wave functions were generated for the calculation of core to valence transition matrix elements[50]. The use of pseudopotentials also results in spectra on energy scales relative to the Fermi level of the respective simulation box and thus the spectra from separate AIMD snapshots are not necessarily on the same absolute energy scale. We therefore shifted the average spectrum of each box such that the oxygen K-edge pre-peak is at 535 eV as it was found in the experiment. This rigid shift was then applied to all individual spectra from the corresponding snapshot. We calculated K-edge spectra for all oxygen atoms from five individual simulation snapshots of the neat water AIMD run resulting in a total of 640 individual oxygen K-edge spectra. For the aqueous TMAO solution, we sampled all oxygen atoms from 50 snapshots of the AIMD trajectory yielding a total of 5400 individual oxygen K-edge spectra, 50 of which stem from TMAO's oxygen atom of TMAO and 5350 spectra from the solvating H_2O molecules. For the aqueous urea solution, we sampled all K-edges from oxygen atoms in 54 individual snapshots, i.e. 54 out of the 5994 K-edge spectra stem from urea's oxygen of urea. For comparison with earlier experimental results[35], the simulations were performed at a finite momentum transfer of 6.8 $Å^{-1}$ and all spectra were convoluted with a Gaussian of 0.65 eV full width at half maximum (FWHM) to account for the finite experimental resolution. As demonstrated in Ref.[39], each oxygen spectrum calculated in this way holds invaluable information about the local atomic environment of the scattering oxygen site.

In addition to the simulations based on snapshots of the AIMD trajectories, we performed oxygen K-edge simulations of hydrous and anhydrous crystalline TMAO[51,52].

2.3 Experimental spectra

All experimental spectra are taken from Ref.[35]. Non-resonant inelastic X-ray scattering spectroscopy is also often called X-ray Raman scattering (XRS) spectroscopy and yields information comparable to soft X-ray absorption spectroscopy, especially so at low values of momentum transfer q[53]. However, since XRS is non-resonant scattering with incident X-rays of much higher energy than the probed excitation energy scales, the measured spectra are practically free of saturation and self-absorption artifacts and the use of hard X-rays offers advantages for the measurement of liquids at well defined temperature and pressure conditions as well as for samples contained in complicated sample environments[54,55]. All spectra were measured with the large solid angle spectrometer at ID20 of the ESRF[56] using milli-q water for the pure water spectra and stochiometric mixtures of milli-q water ($R > 18M\Omega$) with TMAO and urea (both purchased from Sigma Aldrich; TMAO: $C_3H_9NO \cdot 2H_2O$, $> 99.0\%$ purity; urea: CH_4N_2O, anion trace (Cl^-) < 5 ppm). All solutions were measured using a miniature liquid flow cell[57]. Spectra taken from Ref.[35] are normalized to equal area between 526.0 to 550.0 eV.

2.4 Structure characterization

In order to explore the local geometric atomic environment of the scattering oxygen atoms, we define a selection of structural parameters as follows.

2.4.1 Hydrogen bonds

We consider a molecule to be hydrogen bonded subject to geometric criteria as defined in Refs.[58,59] and utilized also in Ref.[39]. We consider hydrogen bonding via two oxygen atoms (either from an H_2O molecule or the O atom of TMAO or urea) if the oxygen-oxygen separation is less than 3.5 Å and the hydrogen-donor-acceptor angle is less than or equal to 30°. Hydrogen

donor bonds via urea's amino group are similarly considered if the nitrogen-oxygen distance is less than 3.5 Å and the hydrogen-donor-acceptor angle is less than or equal to 30°. Beyond the presented parameters, there have been other approaches used to charactize the hydrogen-bonding between water and TMAO[29,30].

2.4.2 Urea/TMAO solvation by H_2O molecules

The zwitterionic TMAO molecule (see Fig. 1) is composed of a hydrophilic N=O unit and three hydrophobic CH_3 (methyl) groups. We separate the hydration water molecules of these two moieties subject to geometric criteria. We consider a water molecule to hydrate the NO-head-group (hydrophilic group) if its oxygen atom is found within a cone of 120° opening centered around the intra-TMAO-molecular N-O separation vector. Otherwise the H_2O molecule is considered to hydrate the CH_3-groups (hydrophobic methyl groups). This separation is schematically depicted in Fig. 1 b) (left).

For the direct comparison between the urea and TMAO solutions, we use a similar classification scheme for both solutions. Water molecules within a cone of 120° opening around the intra-urea-molecular C-O separation vector are considered to hydrate urea's carbonyl group (CO), whereas water molecules that are found outside of this cone are considered to hydrate the amino groups (NH_2).

2.4.3 Hydration shells

We define the number of molecules in the solvation shells around the urea and TMAO molecules based on distance criteria. We separate the solvent molecules into 2 groups: water molecules hydrating the TMAO NO head group (CO head group for urea) and water molecules hydrating the CH_3-groups of TMAO (NH_2 groups of urea) as described in the previous section.

We define the hydration shells of these two groups based on the radial distribution functions (RDF) calculated separately for the hydrophilic and hydrophobic part of TMAO. For the hydrophilic side, we use the position of the weak minima of the O_{TMAO}-O_W RDF at 3.3, 5.4, 7.7 Å, defining four shells, where the fourth shell is defined by all water molecules that can be found beyond 7.7 Å. The cut-off distances on the hydrophilic side of the TMAO molecule are measured from the oxygen atom of TMAO. On the hydrophobic side, we use the approximate position of weak minima of the C_{TMAO}-O_W RDF at 4.7, 7.0 Å, i.e. the limited extent of the simulation box allows us to define three shells. Here, the cut-off distances are measured from the carbon atom closest to the respective water oxygen atom. The partial RDFs are shown in Fig. 1 c). For the analysis of the aqueous urea simulations, we use the same cut-offs as for TMAO, but we measure distances with respect to the N atom of the amino groups (NH_2) and with respect to the oxygen atom of the CO head group. The principle of separation into the two regional groups as well as the separation into the different hydration shells is illustrated in Fig. 1 b). Here, cut-offs for the TMAO (urea) molecule on the carbonyl (nitroso) side are depicted as light blue dashed lines and those on the methyl (amino) side as green (red) dashed lines. We have used and tested other cut-off schemes and distance criteria, which all yield results that are qualitatively comparable. The sizes of the cubic simulation boxes $a_{TMAO} = 14.9382$ Å and $a_{urea} = 14.9984$ Å imply that the fourth solvation shell may overlap slightly with the fourth solvation shell of the respective solute's mirror image due to the periodic boundary conditions.

In addition to these two groups we define the set union of the two regional groups for the first three hydration shells (denoted as all H_2O) in order to allow for discussions considering hydration of the whole molecule in terms of shell structure and isotropic distance from the respective molecule. A table summarizing the number of molecules in these different shells averaged over all simulation snapshots is shown in the table 1.

3 Results

A side by side comparison of the experimental and simulation results is shown in Fig. 2, where the previously published experimental K-edge data of pure water and 2M solutions of TMAO and urea are shown in part a) and the computed spectra are shown in part b). Part c) and d) show the respective difference spectra between pure water and the aqueous solutions. The three main spectral features, pre-edge (I), main-edge (II), and post-edge (III) are highlighted in grey. The overall accordance of theory and experiment is remarkable as evident especially from a comparison of the difference spectra for energy losses above 535 eV.

The computed spectra are compressed along the energy loss axis compared to the experimental spectra, due to the failure of density functional theory to accurately predict the band gaps of insulators. This phenomenon is well known[60] and can in principle be corrected for, e.g. by using a GW-type correction. However, the computational cost of such simulations for the used large simulation boxes is beyond current computational limits. Likewise, at energy losses beyond 547 eV, the calculated spectrum of pure water shows less spectral weight than the ones of the aqueous solutions. This deficiency is due to the finite number of unoccupied states used in the simulation of the large water box. We therefore limit the performed analysis to the near edge structure below 547 eV.

In order to examine the influence of the osmolyte molecule on the hydrating water molecules, we consider the oxygen K-edge of water molecules found within the different coordination shells as defined above. Averaged spectra from of the hydrohilic region of the solutes (all shells only shown in the SI as discussed later) are shown in comparison to the calculated spectrum of pure water in Fig. 3 for TMAO in part a), and for urea in part b). By far the strongest influence on the shape of the spectrum are found for the water molecules immediately hydrating the NO- and CO-groups of TMAO and urea, respectively. For TMAO a lack of the characteristic water pre-edge, a prominent loss of intensity in the main-edge region and an enhanced post-edge are observed. The variations found in the according spectra from the shells hydrating the CO head group of urea are much smaller, but a small decrease in main- and increase in post-edge is observable for the spectrum of the first shell. The spectroscopic fingerprints from the the two solvents are therefore qualitatively similar for the two solutes, but weaker for urea.

The effects of hydration of TMAO's methyl- and urea's amino-groups are much smaller (see SI Fig. 9). Here, the overall shape

of the spectra are more or less unchanged with small alterations in the relative weight of pre-, main-, and post-edge.

In summary, the spectral changes observed as a function of distance from the differently and partially charged groups of the TMAO and urea molecules, apart from the signatures of the first shell, are small as are the differences between the different experimental spectra. We therefore will take a closer look at spectra extracted from a series of experimental data via a non-negative matrix factorization (NNMF) approach[35]. The NNMF approach was performed using three components and their respective weights to best describe all spectra of the full concentration series: the fixed experimental spectra of water, a polycrystalline powder sample in the case of urea and a simulated spectrum of an anhydrous TMAO polycrystal, as well as a freely variable spectrum (hereafter referred to as 'free component spectrum' (FCS)), the shape of which was optimized during the procedure. In case of the hydrous TMAO powder sample, the oxygen contribution of the H_2O molecules complicates the NNMF analysis. Therefore, we instead used a simulated spectrum based on the crystal structure of the anhydrous crystal for the analysis (see SI for a justification of this procedure). The FCS spectra were interpreted as those spectra best representing the change of the measured oxygen K-edges upon solvation of TMAO and urea, i.e. the FCS spectra best describe the influence of the TMAO (urea) molecules on the surrounding water molecules. The procedure of finding the FCS bases on its optimization together with weights for all three spectral components such that data from a series of concentrations is best described.

Fig. 4 shows the FCS spectra extracted from the experimental data in comparison to the experimental spectrum of pure water in part a) (top) for TMAO and in part b) (top) for urea. At the bottom of the same panels we show the simulated spectrum of pure water (black dashed lines, bottom) in direct comparison with the spectra of the first shell around the NO-group in TMAO and the CO-group of urea (solid turquoise and solid red line, bottom). These first shell spectra starkly resemble those of the experimental FCS spectra with a depleted main- and increased post-edge. As in the experiment, these changes are greater for TMAO than for urea. Solely, the region of the pre-edge and the π^*-peak of urea's and TMAO's oxygen atom (energy losses < 536 eV) are not represented by the spectrum of the first shell water molecules but originate from the change in spectral shape of TMAO's and urea's oxygen atom upon hydration.

Finally, in Fig. 5 we summarize the total number of hydrogen bonds per water molecule (part a)) and the mean hydrogen bond angle (part b)) found in the TMAO AIMD trajectory and the according trajectory of aqueous urea (part c) and d)). The parameters are compared to those found for the pure water trajectory (dashed grey lines). Hydrogen bonds are well defined according to the named geometrical criteria even in the vicinity of the solute molecule, and their number was shown to correlate with the shape of the oxygen K-edge spectrum of pure water[39]. The deviation from the values of pure water are largest in the first shell but the effect has notable contributions from other shells as well. The formation of strong hydrogen bonds between water molecules and the NO-group of TMAO on the hydrophilic side (part a)) leads to an enhancement of the number of H-bonds on that side, whereas the number of hydrogen bonds on the hydrophobic side is depleted in comparison to pure water. This is unique to TMAO and we do not find a similar enhanced number of hydrogen bonds amongst water molecules hydrating urea's CO-group. The change in hydrogen bond angles as a function of distance from the solvated molecule is similar around TMAO and urea molecules with slightly more straightened bonds in the case for TMAO. In both cases, the solvation of the molecules induces higher bond directionality on the hydrophilic side than found in the AIMD trajectory of pure water.

4 Discussion

4.1 X-ray spectroscopy at the oxygen K-edge

The K-edge excitation spectrum is a formidable probe of the local electronic and structural environment of the absorbing oxygen atom. Recent computational and experimental work showed that structural properties such as the number of hydrogen bonds and the deviation from tetrahedrality are correlated with the shape of the excitation spectrum[38,39,61,62]. As such, the pre-edge structure around an excitation energy of 535 eV is prominent if the water-water hydrogen bond network is highly disrupted[61]. Likewise, the main-edge centered around 539 eV is prominent in highly disordered environments, while the post edge at around 541 eV is prominent in a well ordered and strongly hydrogen bonded environment, for example found in the low pressure crystalline ice phases[63,64]. These observations must be viewed as structural fingerprints of a statistical ensemble, because notable variation (scatter) exists in the structural parameter – intensity relation[39].

In the present study, the situation is slightly more complicated as the oxygen atoms of TMAO and urea add an additional component to the measured K-edge spectrum. As was shown in the earlier study, this oxygen atom is most evident by the increased intensity at 534 eV[35], which is due to the presence of the double bond (N=O in TMAO and C=O in urea) resulting in a strong $1s$ to π^* excitation feature just below the onset of the oxygen K-edge of the water solvent (see SI Fig. 6). However, at the probed low osmolyte concentrations, the main- and post-edge contribution of TMAO's and urea's oxygen atom to the ensemble average over all excited oxygen sites as shown in Fig. 2 is relatively small and is represented mostly by the intensity at 534 eV energy loss.

An influence of TMAO on the structure of water is well reported, either as an influence on a larger or bulk scale based on an observed red-shift of the OH vibration spectrum[65] and a strengthening of the water-water hydrogen bond network[6,66], or as a strong local association of three water molecules by the hydrophilic NO-group. Latter was already reported for the used AIMD simulations[40] and is in line with with earlier classical force-field simulations[67,68] and experimental work[26,69,70].

Urea, despite the earliest referrals to as a water structure breaker[71], is generally viewed as well fitting into the water network[72]. An influence on the second water-water neighbor shell was reported on the basis of diffraction experiments[73], but most recent MD simulation studies reveal that urea, like TMAO, slows down the water dynamics and exhibits kosmotropic properties

similar to TMAO but to a lesser extent[32]. This is consistent with recent findings of a preferential exclusion of urea from a polymer surface at low urea concentrations in a classical MD simulation.[74].

From the ensemble averaged spectra the discrimination between the local and itinerant effects of hydration of TMAO and urea is impossible, because all oxygen atoms (from both the solvent and the solute) contribute to the spectrum. However, the MD simulations yield access to local structural information around each excited oxygen site via the spectrum simulations. The analysis shown in Fig. 3 demonstrates the strong influence of the immediate surrounding of the hydrated solute molecules on the shape of the oxygen K-edge. Moreover, this analysis allows us to observe the differences between the molecules hydrating the two sides of the polar osmolyte molecules.

On the hydrophilic side of TMAO, the strong hydrogen bonding of three water molecules[40] form a well defined shell with well defined next-neighbor distances. It is reasonable to expect that these well defined hydration shells result in strong spectral weight in the post-edge region and a depleted main- and pre-edge (Fig. 3 a)), analogously to the case of pure water and ice, for which it was shown that the formation of well defined nearest neighbor shells results in well defined potential barriers for a shape resonance[38]. This is reflected in the spectral differences with respect to the average water spectrum on the hydrophilic side of TMAO. The influence of TMAO's methyl groups on the shape of the K-edge spectrum (SI Fig. 9 a)) is much weaker and no strong spectral variation can be observed.

The situation around the urea molecule is qualitatively similar, but to a much smaller extent. We observe a slightly depleted main-edge and a slightly enhanced post-edge for the spectra of the first shell molecules around the carbonyl group (Fig. 3 b)). This observation is in clear contrast to the proposed concept of urea as having an opposite effect on the water structure when compared to TMAO[11]. The structural alterations of water when compared to pure neat water are reflected in the structural parameters extracted from the AIMD simulations, which are shown in Fig. 5 and which support the qualitative assessment based on the shape of the K-edge spectra.

For TMAO, the total number of hydrogen bonds is increased on the hydrophilic side as TMAO's oxygen atom forms strong hydrogen bonds with the solvent molecules. The number of hydrogen bonds is decreased on the hydrophobic side of the TMAO molecule since the methyl groups do not form hydrogen bonds with any water molecules. The strong hydrogen bonding between the H_2O solvent molecules and the hydrophilic head group of the TMAO molecule is also evident by a stark decrease in the mean hydrogen bond angle (see Fig. 5 b)), showing that these bonds are more directional in line with the reported formation of strong TMAO-$(H_2O)_3$ complexes that exhibit extraordinarily long life times and induce slower water dynamics[26,29,30,32]. In the vicinity of the hydrophobic methyl groups, the difference in mean angle with respect to pure water is small. Distinctively slower dynamics for water molecules interacting with the hydrophobic part of the TMAO molecule in comparison to those found in pure water have also been reported[26,75]. However, we note that the observable oxygen K-edge spectra are not sensitive to the dynamics in the electronic ground state, but only the statistical distribution of configurations in the statistical ensemble. This is due to the extremely short duration of an inelastic X-ray scattering event.

For urea, the number of hydrogen bonds in the vicinity of the carbonyl head group are similar to the numbers found in pure bulk water (Fig. 5 c)), however, as found around TMAO's NO-group the hydrogen bonds are more directional (smaller mean H-bond angle, Fig. 5 d)). In the vicinity of the amine groups, the number of hydrogen bonds is depleted and the bond angles are comparable to those in bulk water. These results suggest that a somewhat similar hydration scenario for urea and TMAO exists. Even though TMAO has a much stronger influence on the hydration water molecules and consequently the oxygen K-edge spectra, kosmotropic properties in aqueous solution should be attributed to both osmolytes in accord with recent force-field MD simulations[32]. A drastic effect on the second water-water hydration shell, as observed by neutron scattering[73], cannot be inferred from the structural parameters extracted here and the overall shape of the oxygen K-edge.

As a function of distance from the osmolyte molecules, the strongest effects both in terms of the structural parameters extracted directly from the AIMD simulation and in terms of the shape of the oxygen K-edge spectra are found within the immediate vicinity of the NO- and CO-groups (Fig.s 7 and 8 in the SI). On the opposite side (around the CH_3- and NH_2-groups) we observe a small enhancement of the pre-edge for the 1st shell (see SI Fig. 9), an indication of slightly enhanced numbers of broken donated H-bonds of the water molecules.

A congruent picture emerges. A strong short-range interaction on TMAO's hydrophilic side with mostly three strong and directional hydrogen bonds induces local order in the direct vicinity of the hydrophilic part of the osmolyte and a small reduction of hydrogen bonds in the immediate vicinity of the hydrophobic side[26,75]. Slight changes in the shape of the oxygen K-edge spectra, however, seem to persist to well into the highest coordination shells probed within the small simulation cell. Therefore, our spectra do not entirely rule out long-range interactions beyond the first few shells[6]. Similar kosmotropic interactions can be attributed to urea, but their strength and extent is much reduced when compared to TMAO, explaining the referral to urea as fitting well into the water network[72].

The oxygen K-edge excitation spectra are clearly sensitive to these hydration effects and, most importantly, details of the very local surroundings of the solutes can be extracted directly from the experimental spectra via the NNMF of a series of measurements of differently concentrated osmolyte solutions. The extracted FCSs seem to be directly comparable to the spectra calculated from snapshots of AIMD trajectories. In fact, the extracted FCSs represent the most drastic changes in spectral shape induced by the hydration of the osmolyte molecules.

4.2 Relations to the protein (de-)stabilization mechanisms

In the following, we are relating the presented results from combined experimental XRS spectroscopy and density functional the-

ory to the different proposed mechanisms for protein (de-) stabilization reported in the recent literature.

Based on our results on the effect of the osmolyte on the local water structure, a long-range and water-mediated interaction seems unlikely for the stabilization through TMAO and the destabilization by urea. TMAO affects the water structure strongly for a few hydration layers. A clear directional dependence is confirmed by the AIMD simulations that are in line with our comparison between experimental findings and spectral calculations, which solves recent contradictory findings[10,76]. This might further be in accord with preferred-hydration-by-preferred-binding mechanisms[19–21,23,24,77]: TMAO strongly affects the water molecules that immediately hydrate it and thus in the proximity to the protein surface. Therefore, the macromolecules are more hydrated while at the same time the TMAO molecules are close to the protein's surface. In this scenario, the interplay between proteins and TMAO is relatively short-ranged and water mediated. A similar finding has been reported recently for a MD simulation of a protein in aqueous TMAO solution[78].

Of course, the strong potential of TMAO to accept hydrogen bonds might also contribute to alternative stabilization mechansisms such as preferred exclusion or direct binding and a direct correlation between the impact of the studied osmolytes on the structure of water and the impact of the presence of these osmolytes on the stability of macromolecules and proteins is not indisputable[79].

Longer-ranged interactions observable in some experiments and simulations alter the water network in more distant coordination shells but this effect may not be congruent with the protein's hydration water and the presented findings.

We would like to note that such a short ranged water mediated scenario is also in line with the observation that TMAO at low pH values (pH 4) loses its ability to stabilize macromolecules[80]. Even a slightly different charge state of TMAO's NO-group is likely to change the strong interaction with water molecules in its proximity. As a consequence, the hydration properties at the protein surface will be different, possibly not any more favorable for a water-moderated TMAO–protein interaction. Such a hydration-water mediated stabilization mechanism is indeed observed for model polymers[19–21,23,24]. In a somehow similar spirit, Liao *et al.* considered TMAO as acting as a surfactant for the heterogeneous surface of proteins, resulting in its stabilizing properties[22]. This mechanism can also explain the increase of the attractive character of the protein-protein interaction as has been observed at high TMAO concentrations[9,34,81]. In the preferred-hydration-by-preferred binding framework this interaction can be understood as being mediated by water-TMAO bridges, resulting in an effective protein-water-TMAO-TMAO-water-protein arrangement. Somehow similar as reported for polymer systems, the basis for stabilization (preferred intramolecular interactions) can also lead to aggregation/association (preferred intermolecular interactions).

As for the destabilizing influence of urea on proteins and macro-molecules, the slight kosmotropic behavior that, in effect, seems similar to that of TMAO but much smaller in magnitude is in contrast with an indirect and water-mediated mechanism as suggested in early work[71,82]. A direct interaction with the proteins' backbone in accordance with more recent literature[4,83–85] is more likely at high urea concentrations based on how urea interacts with its immediate surrounding in the studied aqueous solutions. Moreover, the (weak) kosmotropic effect of urea can be related to the reported finding that for low concentrations even urea can lead to a stabilization[74,86]. The number of hydrogen bonds per water molecule and the mean hydrogen bond angle found in the AIMD simulations for both osmolytes reach similar values already for the second shell. This points to the conclusion that the opposite biological effect of the two osmolytes on proteins (if due to osmolyte-water-protein interactions only) is limited to a similar spatial extent. This restriction means direct interaction, or interaction mediated only by a single water solvent layer. This spatial restriction is consistent with a direct interaction of osmolyte and macromolecule, or an interaction mediated only by a single water solvent layer.

Further insight into the protein stabilization and destabilization mechanisms requires deeper investigation of the TMAO-urea interaction and their combined effect on the water network. Partial radial distribution functions from neutron diffraction pointed to a direct association of TMAO and urea molecules via hydrogen bonding[69,70], however, newer combined AIMD and experimental work suggests association between TMAO and urea via the hydrophobic moieties[87].

Summarizing, in the context of the presented data and the recent literature, the ability of TMAO to stabilize and of urea to destabilize proteins and macromolecules seems to be based on their respective ability to interact with their respective (effectively low number of) hydrating water molecules: For low concentration both TMAO and urea locally interact with water molecules in their close proximity.

With increasing concentration, i.e. decreasing number of bulk water molecules per osmolyte molecule and the concomitant decrease in the number of water molecules available per protein, urea may fail to maintain its well-hydrated state, leading to possible favorable interactions with the internal protein backbone at high osmolyte concentrations that otherwise stabilizes the denatured state. Conversely, under such conditions, the strong TMAO-water interaction leaves TMAO fully hydrated that could manifest as preferred-hydration-by-preferred-binding toward the folded protein surface resulting in a possible destabilisation of the denatured state and the observed increase in stability and/or a propensity toward self-association in solution. Upon weakening the strong TMAO-water interaction, for example by changing the pH of the solution[80], TMAO loses it's protein stabilizing abilities. Such a scenario would lead to a systematic trend when correlating the cosolvent-water interaction with the (de)stabilizing influence on proteins and macromolecules. Obviously, entropic influences such as excluded volume have to be taken into account.

5 Conclusions

We used oxygen K-edge spectrum calculations from structures of *ab initio* molecular dynamics simulations[40–42] of pure water and aqueous solutions of TMAO and urea in comparison to experimental data from non-resonant inelastic X-ray scattering in order

to study the microscopic details of the solute-solvent interactions in these solutions. We observed a remarkable agreement between the experiment and the simulations.

Simulated spectra of water molecules in the direct vicinity of the solutes' hydrophilic groups (NO in TMAO, CO in urea) closely resemble spectra extracted from a series of measurements of differently concentrated osmolyte solutions via a non-negative matrix factorization approach. This reveals a direct access to the hydration of TMAO, urea and possibly other small solutes via oxygen K-edge spectroscopy and manifests the relative importance of these first few hydration layers for the overall change in spectral shape observed in the experimental spectra of the statistical ensemble averages.

Further exploration of the structural simulations reveals that both TMAO and urea have an overall kosmotropic effect on their immediate surroundings, however, the influence of urea is much smaller than that of TMAO.

For a water-mediated mechanism of the biologic effects of the osmolytes on protein stability it is expected that the two osmolytes should alter the water structure differently. In the AIMD simulations, which are fully consistent with experimental XRS data, as demonstrated here, these structural changes were observed to stem mainly from the first solvation shell. The presented results therefore support the conclusion that one water layer at most is involved for such a mechanism. Furthermore, the findings render a water-mediated protein destabilization by urea unlikely. The very strong interaction between water and TMAO's amine-oxide group allows for speculations that preferred-hydration-by-preferred-binding may play a role in the mechanisms leading to the stabilization of proteins and macromolecules by TMAO.

The combination of the experimentally accessible ensemble averaged oxygen K-edge in combination with *ab initio* molecular dynamics simulations and site-by-site spectrum calculations is extremely powerful to unravel the detailed and local effects of hydration in aqueous solutions. Signatures found in the experimental data can thus be readily interpreted in terms of local atomic structures. The interplay between multiple TMAO or urea molecules as well as their mutual influence in ternary water-TMAO-urea solutions is subject of recent experimental[88,89] and simulation[32,90–93] studies. Confrontation of these recent results with spectroscopic oxygen K-edge data would certainly allow further insights into these relevant solutions.

Acknowledgements

We are grateful to S. Imoto and D. Marx for providing the *ab initio* molecular dynamics simulation trajectories. We are thankful to Iina Juurinen and Jens Smiatek for fruitful discussions. The European Synchrotron Radiation Facility is acknowledged for providing computing resources. MAS thanks the Röntgen-Ångström cluster project "TT-SAS" (BMBF project number 05K16YEA). ME and CS acknowledge funding via BMBF project number 05K16PE1 and thank Metin Tolan for supporting these activities.

Table 1 Number of H_2O molecules in the different hydration shells for TMAO (top) and urea (bottom). All numbers represent mean values over all used structural snapshots. The errors represent standard deviations from the mean.

shell (TMAO)	total	NO-group	CH_3-groups
all shells	107.0 ± 0.0	27.9 ± 2.1	79.1 ± 2.1
shell 1	19.2 ± 1.5	3.0 ± 0.2	16.2 ± 1.6
shell 2	40.2 ± 2.8	7.2 ± 1.1	33.0 ± 2.7
shell 3	40.8 ± 2.9	10.9 ± 2.0	29.9 ± 2.7
shell 4	6.9 ± 1.8	6.9 ± 1.8	0.0 ± 0.0

shell (urea)	total	CO-group	NH_2-groups
all shells	110.0 ± 0.0	27.9 ± 2.6	82.1 ± 2.6
shell 1	16.5 ± 1.4	2.7 ± 0.5	13.8 ± 1.4
shell 2	39.3 ± 2.5	6.7 ± 1.3	32.7 ± 2.7
shell 3	46.4 ± 3.4	10.8 ± 2.0	35.6 ± 3.0
shell 4	7.8 ± 2.9	7.8 ± 2.9	0.0 ± 0.0

Supporting information

In Fig. 6 a) we report oxygen K-edge spectra of a TMAO molecule in vacuum (bare molecule) and of TMAO molecules hydrogen bonded to two, three, and four water molecules, respectively. Latter spectra were calculated based on the different snapshots from the AIMD simulation. In the vast majority of analyzed snapshots, the TMAO molecule is found to hydrogen bond to three water molecules.

Fig. 6 b) shows a similar analysis for urea, i.e. the oxygen K-edge spectrum of a bare urea molecule and spectra of the oxygen K-edge spectra of urea from the AIMD simulations. The distribution of number of hydrogen bonds is broader and almost equal amounts of urea molecules are bound to two and three water molecules via hydrogen bonding.

In addition to the total number of hydrogen bonds and the mean hydrogen bond angle (Fig. 5) presented in the main text, we quantified the tetrahedrality of the first hydration shell in the pure water snapshots and the hydration water molecules of the aqueous TMAO solutions using the deviation from the perfect $(H_2O)_5$ tetrahedra that can be found in the low pressure cyrstalline ice phases. Both, the angular deviation and the distance deviation as defined in Ref.[39] are considered. These values, together with the oxygen-oxygen coordination numbers of the hydration waters, are reported in Fig. 7 and Fig. 8. Obviously, these values are biased do to the presence of the TMAO molecule that is not accounted for in the evaluation of the respective parameters.

In table 1, we summarize the number of H_2O molecules in the different hydration shells for TMAO (top table) and Urea (bottom table), respectively. The numbers are shown as averages over the used trajectory snapshots and errors represent standard deviations from the mean.

In Fig. 9, we compare the K-edge spectra of the hydrating water molecules as a function of distance from the TMAO and urea molecule.

TMAO is very hygroscopic and therefore we used a calculated

reference instead of the experimental data from Ref.[35]. Fig. 10 a) shows a comparison between simulated spectra of a hydrous and anhydrous crystalline TMAO with that of the experimental reference spectum from Ref.[35]. Both calculated spectra were convoluted with a Gaussian of 2.5 eV full width at half maximum as the spectrum of the hydrous simulation then compares best to the measured spectrum. In part b) we show the results of a series of non-negative matrix factorizations, each of which uses a different reference for the pure TMAO spectrum as shown in part b). The resulting free component spectra are very similar as the factorization is based on a whole series of experimental spectra of differently concentrated TMAO solutions and, even at the highest studied concentrations, the spectral weight stemming from H_2O is much greater than that stemming from TMAO's oxygen atom.

Since urea is much less hygroscopic than TMAO, we used the experimentally measured pure urea spectrum as reference.

Notes and references

1 P. Yancey, *Am. Zool.*, 2001, **41**, 699–709.

2 P. Yancey, *J. Exp. Biol.*, 2005, **208**, 2819–2830.

3 P. Yancey, M. Clark, S. Hand, R. Bowlus and G. Somero, *Science*, 1982, **217**, 1214–1222.

4 D. Canchi and A. Garcia, *Annu. Rev. Phys. Chem.*, 2013, **64**, 273–293.

5 I. Baskakov and D. Bolen, *J. Biol. Chem.*, 1998, **273**, 4831–4834.

6 Q. Zou, B. J. Bennion, V. Daggett and K. P. Murphy, *J. Am. Chem. Soc.*, 2002, **124**, 1192–1202.

7 C. Mello and D. Barrick, *Protein Sci.*, 2003, **12**, 1522–1529.

8 C. Krywka, C. Sternemann, M. Paulus, M. Tolan, C. Royer and R. Winter, *Chem. Phys. Chem.*, 2008, **9**, 2809–2815.

9 M. Schroer, Y. Zhai, D. Wieland, C. Sahle, J. Nase, M. Paulus, M. Tolan and R. Winter, *Angew. Chem., Int. Ed.*, 2011, **50**, 11413–11416.

10 T. Ohto, J. Hunger, E. Backus, W. Mizukami, M. Bonn and Y. Nagata, *Phys. Chem. Chem. Phys.*, 2017, **19**, 6909–6920.

11 B. J. Bennion and V. Daggett, *Proc. Natl. Acad. Sci. U. S. A.*, 2003, **100**, 5142–5147.

12 G. A. de Oliveira and J. L. Silva, *Proc. Natl. Acad. Sci. U. S. A.*, 2015, **112**, E2775–E2784.

13 D. R. Canchi, P. Jayasimha, D. C. Rau, G. I. Makhatadze and A. E. Garcia, *J. Phys. Chem. B*, 2012, **116**, 12095–12104.

14 Z. Su, F. Mahmoudinobar and C. L. Dias, *Phys. Rev. Lett.*, 2017, **119**, 108102.

15 B. J. Bennion and V. Daggett, *Proc. Natl. Acad. Sci. U. S. A.*, 2004, **101**, 6433–6438.

16 M. Auton and D. W. Bolen, *Proc. Natl. Acad. Sci. U. S. A.*, 2005, **102**, 15065–15068.

17 P. Bruzdziak, A. Panuszko and J. Stangret, *J. Phys. Chem. B*, 2013, **117**, 11502–11508.

18 T. O. Street, D. W. Bolen and G. D. Rose, *Proc. Natl. Acad. Sci. U. S. A.*, 2006, **103**, 13997–14002.

19 F. Rodríguez-Ropero, P. Rötzscher and N. F. van der Vegt, *J. Phys. Chem. B*, 2016, **120**, 8757–8767.

20 J. Mondal, G. Stirnemann and B. Berne, *J. Phys. Chem. B*, 2013, **117**, 8723–8732.

21 J. Mondal, D. Halverson, I. T. Li, G. Stirnemann, G. C. Walker and B. J. Berne, *Proc. Natl. Acad. Sci. U. S. A.*, 2015, **112**, 9270–9275.

22 Y.-T. Liao, A. C. Manson, M. R. DeLyser, W. G. Noid and P. S. Cremer, *Proc. Natl. Acad. Sci. U. S. A.*, 2017, **114**, 2479–2484.

23 M. Schroer, J. Michalowsky, B. Fischer, J. Smiatek and G. Grübel, *Phys. Chem. Chem. Phys.*, 2016, **18**, 31459–31470.

24 L. Martínez and S. Shimizu, *J. Chem. Theory Comput.*, 2017, **13**, 6358–6372.

25 A. Panuszko, P. Bruzdziak, J. Zielkiewicz, D. Wyrzykowski and J. Stangret, *J. Phys. Chem. B*, 2009, **113**, 14797–14809.

26 J. Hunger, K.-J. Tielrooij, R. Buchner, M. Bonn and H. Bakker, *J. Phys. Chem. B*, 2012, **116**, 4783–4795.

27 L. Larini and J.-E. Shea, *J. Phys. Chem. B*, 2013, **117**, 13268–13277.

28 J. Towey, A. Soper and L. Dougan, *Faraday Discuss.*, 2013, **167**, 159–176.

29 K. Usui, J. Hunger, M. Sulpizi, T. Ohto, M. Bonn and Y. Nagata, *J. Phys. Chem. B*, 2015, **119**, 10597–10606.

30 G. Stirnemann, E. Duboué-Dijon and D. Laage, *J. Phys. Chem. B*, 2017, **121**, 11189–11197.

31 F. Lehmkühler, Y. Forov, M. Elbers, I. Steinke, C. Sahle, C. Weis, N. Tsuji, M. Itou, Y. Sakurai, A. Poulain *et al.*, *Phys. Chem. Chem. Phys.*, 2017, **19**, 28470–28475.

32 E. Oprzeska-Zingrebe and J. Smiatek, *J. Phys. Chem. B*, 2019, **123**, 4415–4424.

33 C. Sahle, M. Schroer, C. Jeffries and J. Niskanen, *Phys. Chem. Chem. Phys.*, 2018, **20**, 27917–27923.

34 K. Julius, J. Weine, M. Berghaus, N. König, M. Gao, J. Latarius, M. Paulus, M. Schroer, M. Tolan and R. Winter, *Phys. Rev. Lett.*, 2018, **121**, 038101.

35 C. Sahle, M. Schroer, I. Juurinen and J. Niskanen, *Phys. Chem. Chem. Phys.*, 2016, **18**, 16518–16526.

36 C. Sahle, J. Niskanen, K. Gilmore and S. Jahn, *J. Electron Spectrosc. Relat. Phenom.*, 2018, **222**, 57–62.

37 J. Niskanen, C. J. Sahle, I. Juurinen, J. Koskelo, S. Lehtola, R. Verbeni, H. Müller, M. Hakala and S. Huotari, *J. Phys. Chem. B*, 2015, **119**, 11732–11739.

38 J. Niskanen, M. Fondell, C. Sahle, S. Eckert, R. Jay, K. Gilmore, A. Pietzsch, M. Dantz, X. Lu, D. McNally *et al.*, *Proc. Natl. Acad. Sci. U. S. A.*, 2019, **116**, 4058–4063.

39 J. Niskanen, C. Sahle, K. Gilmore, F. Uhlig, J. Smiatek and A. Föhlisch, *Phys. Rev. E*, 2017, **96**, 013319.

40 S. Imoto, H. Forbert and D. Marx, *Phys. Chem. Chem. Phys.*, 2015, **17**, 24224–24237.

41 C. Hölzl, P. Kibies, S. Imoto, J. Noetzel, M. Knierbein, P. Salmen, M. Paulus, J. Nase, C. Held, G. Sadowski *et al.*, *Biophys. Chem.*, 2019, **254**, 106260.

42 D. Marx and J. Hutter, *Ab Initio Molecular Dynamics: Theory and Implementation*, Cambridge University Press, Cambridge, 2009.

43 B. Hammer, L. Hansen and J. Nørskov, *Phys. Rev. B*, 1999, **59**,

7413.
44 S. Grimme, J. Antony, S. Ehrlich and H. Krieg, *J. Chem. Phys.*, 2010, **132**, 154104.
45 R. Jonchiere, A. Seitsonen, G. Ferlat, A. Saitta and R. Vuilleumier, *J. Chem. Phys.*, 2011, **135**, 154503.
46 J. Vinson, J. Rehr, J. Kas and E. Shirley, *Phys. Rev. B*, 2011, **83**, 115106.
47 K. Gilmore, J. Vinson, E. Shirley, D. Prendergast, C. Pemmaraju, J. Kas, F. Vila and J. Rehr, *Comput. Phys. Commun.*, 2015, **197**, 109–117.
48 P. Giannozzi, S. Baroni, N. Bonini, M. Calandra, R. Car, C. Cavazzoni, D. Ceresoli, G. Chiarotti, M. Cococcioni, I. Dabo *et al.*, *J. Phys.: Cond. Matt.*, 2009, **21**, 395502.
49 *Quantum ESPRESSO*, 2019, `http://www.quantum-espresso.org`.
50 G. Kresse and D. Joubert, *Phys. Rev. B*, 1999, **59**, 1758.
51 A. Caron, G. Palenik, E. Goldish and J. Donohue, *Acta Crystallogr.*, 1964, **17**, 102–108.
52 T. C. Mak, *J. Mol. Struct.*, 1988, **178**, 169–175.
53 Y. Mizuno and Y. Ohmura, *J. Phys. Soc. Jpn.*, 1967, **22**, 445–449.
54 W. Schülke, *Electron dynamics by inelastic X-ray scattering*, Oxford University Press, 2007, vol. 7.
55 C. Sahle, A. Mirone, J. Niskanen, J. Inkinen, M. Krisch and S. Huotari, *J. Synchrotron Rad.*, 2015, **22**, 400–409.
56 S. Huotari, C. J. Sahle, C. Henriquet, A. Al-Zein, K. Martel, L. Simonelli, R. Verbeni, H. Gonzalez, M.-C. Lagier, C. Ponchut *et al.*, *J. Synchrotron Rad.*, 2017, **24**, 521–530.
57 C. J. Sahle, C. Henriquet, M. A. Schroer, I. Juurinen, J. Niskanen and M. Krisch, *J. Synchrotron Rad.*, 2015, **22**, 1555–1558.
58 W. Chen, X. Wu and R. Car, *Phys. Rev. Lett.*, 2010, **105**, 017802.
59 A. Luzar and D. Chandler, *Phys. Rev. Lett.*, 1996, **76**, 928.
60 K. Burke, *J. Chem. Phys.*, 2012, **136**, 150901.
61 C. J. Sahle, C. Sternemann, C. Schmidt, S. Lehtola, S. Jahn, L. Simonelli, S. Huotari, M. Hakala, T. Pylkkänen, A. Nyrow *et al.*, *Proc. Natl. Acad. Sci. U. S. A.*, 2013, **110**, 6301–6306.
62 C. Sahle, J. Niskanen, C. Schmidt, J. Stefanski, K. Gilmore, Y. Forov, S. Jahn, M. Wilke and C. Sternemann, *J. Phys. Chem. B*, 2017, **121**, 11383–11389.
63 S. T. John, D. M. Shaw, D. D. Klug, S. Patchkovskii, G. Vankó, G. Monaco and M. Krisch, *Phys. Rev. Lett.*, 2008, **100**, 095502.
64 T. Pylkkänen, V. M. Giordano, J.-C. Chervin, A. Sakko, M. Hakala, J. A. Soininen, K. Hämäläinen, G. Monaco and S. Huotari, *J. Phys. Chem. B*, 2010, **114**, 3804–3808.
65 K. A. Sharp, B. Madan, E. Manas and J. M. Vanderkooi, *J. Chem. Phys.*, 2001, **114**, 1791–1796.
66 I. M. Pazos and F. Gai, *J. Phys. Chem. B*, 2012, **116**, 12473–12478.
67 M. Athawale, J. Dordick and S. Garde, *Biophys. J.*, 2005, **89**, 858–866.
68 R. Sarma and S. Paul, *J. Chem. Phys.*, 2012, **137**, 094502.
69 F. Meersman, D. Bowron, A. Soper and M. Koch, *Biophys. J.*, 2009, **97**, 2559–2566.
70 F. Meersman, D. Bowron, A. Soper and M. Koch, *Phys. Chem. Chem. Phys.*, 2011, **13**, 13765–13771.
71 H. S. Frank and F. Franks, *J. Chem. Phys.*, 1968, **48**, 4746–4757.
72 N. Muller, *J. Phys. Chem.*, 1990, **94**, 3856–3859.
73 A. Soper, E. Castner Jr and A. Luzar, *Biophys. Chem.*, 2003, **105**, 649–666.
74 S. Micciulla, J. Michalowsky, M. A. Schroer, C. Holm, R. von Klitzing and J. Smiatek, *Phys. Chem. Chem. Phys.*, 2016, **18**, 5324–5335.
75 Y. Rezus and H. Bakker, *Phys. Rev. Lett.*, 2007, **99**, 148301.
76 D. Bandyopadhyay, Y. Kamble and N. Choudhury, *J. Phys. Chem. B*, 2018, **122**, 8220–8232.
77 J. Rösgen and R. Jackson-Atogi, *Journal of the American Chemical Society*, 2012, **134**, 3590–3597.
78 N. Smolin, V. P. Voloshin, A. V. Anikeenko, A. Geiger, R. Winter and N. N. Medvedev, *Phys. Chem. Chem. Phys.*, 2017, **19**, 6345–6357.
79 J. D. Batchelor, A. Olteanu, A. Tripathy and G. J. Pielak, *Journal of the American Chemical Society*, 2004, **126**, 1958–1961.
80 M. Vigorita, S. Cozzolino, R. Oliva, G. Graziano and P. Del Vecchio, *Biopolymers*, 2018, **109**, e23104.
81 M. Niebuhr and M. H. Koch, *Biophys. J.*, 2005, **89**, 1978–1983.
82 G. Walrafen, *J. Chem. Phys.*, 1966, **44**, 3726–3727.
83 L. Hua, R. Zhou, D. Thirumalai and B. Berne, *Proc. Natl. Acad. Sci. U. S. A.*, 2008, **105**, 16928–16933.
84 W. K. Lim, J. Rösgen and S. W. Englander, *Proc. Natl. Acad. Sci. U. S. A.*, 2009, **106**, 2595–2600.
85 D. R. Canchi, D. Paschek and A. E. Garcia, *J. Am. Chem. Soc.*, 2010, **132**, 2338–2344.
86 A. K. Bhuyan, *Biochemistry*, 2002, **41**, 13386–13394.
87 W. J. Xie, S. Cha, T. Ohto, W. Mizukami, Y. Mao, M. Wagner, M. Bonn, J. Hunger and Y. Nagata, *Chem*, 2018, **4**, 2615–2627.
88 J. Hunger, N. Ottosson, K. Mazur, M. Bonn and H. J. Bakker, *Phys. Chem. Chem. Phys.*, 2015, **17**, 298–306.
89 S. G. Zetterholm, G. A. Verville, L. Boutwell, C. Boland, J. C. Prather, J. Bethea, J. Cauley, K. E. Warren, S. A. Smith, D. H. Magers *et al.*, *J. Phys. Chem. B*, 2018, **122**, 8805–8811.
90 P. Ganguly, T. Hajari, J.-E. Shea and N. F. van der Vegt, *J. Phys. Chem. letters*, 2015, **6**, 581–585.
91 P. Ganguly, N. F. van der Vegt and J.-E. Shea, *J. Phys. Chem. letters*, 2016, **7**, 3052–3059.
92 P. Ganguly, P. Boserman, N. F. van der Vegt and J.-E. Shea, *J. Am. Chem. Soc.*, 2018, **140**, 483–492.
93 X. Teng and T. Ichiye, *J. Phys. Chem. B*, 2019, **123**, 1108–1115.

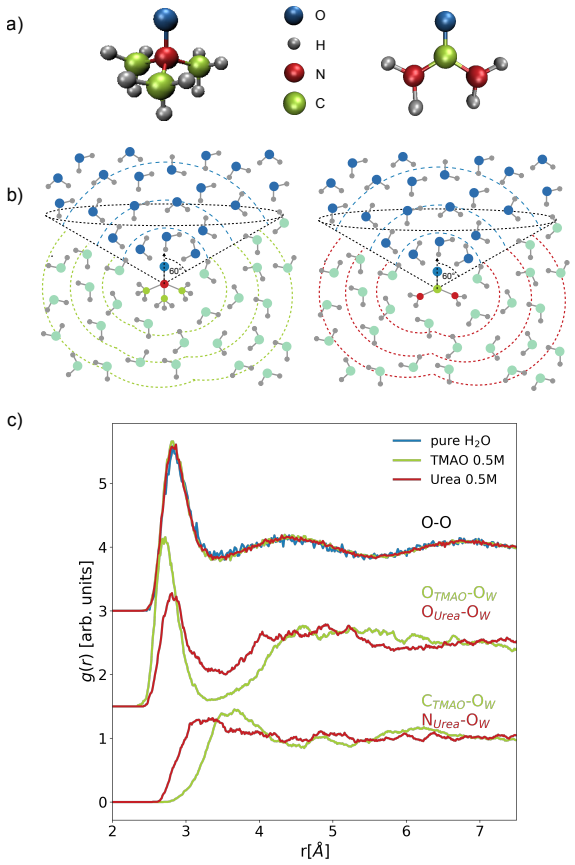

Fig. 1 a) Stick and ball representation of the TMAO (left) and urea (right) molecule. b) Schematic demonstrating our definition separating water molecules that hydrate NO- (CO-) and CH_3- (NH_2-) groups of the TMAO (urea) molecule, respectively, as well as our definition of hydration shells for the NO- (CO-) group (concentric blue dashed circles centered on TMAO's (urea's) oxygen atom) and CH_3- (NH_2-) group (concentric green (red) dashed circle centered on TMAO's carbon (urea's nitrogen) atoms). c) Radial distribution functions from the *ab initio* molecular dynamics simulations. The O_W-O_W RDF from pure water and the osmolyte solutions are shown on the top. The O_{TMAO}-O_W and O_{Urea}-O_W RDFs as well as the C_{TMAO}-O_W and N_{Urea}-O_W RDFs describing the hydration of the two sides of the molecules are shown in the middle and the bottom of part c).

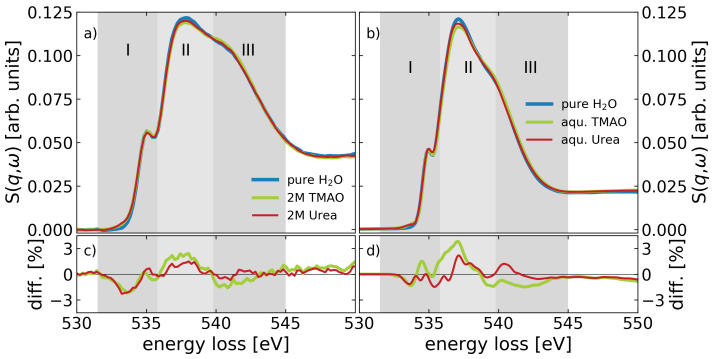

Fig. 2 a) Comparison of experimental XRS spectra of the oxygen K-edge of pure water and 2M solutions of TMAO and urea (data taken from Ref.[35]). b) Average oxygen K-edge spectra from the current BSE simulations of pure water and the aqueous TMAO and urea solutions. The differences between the pure water spectrum and the spectra of the solutions are shown for the experimental and simulation data in part c) and d), respectively. The grey shaded areas indicate the main spectral features of the oxygen K-edge of water and aqueous solutions: pre-edge (I), main-edge (II), and post-edge (III).

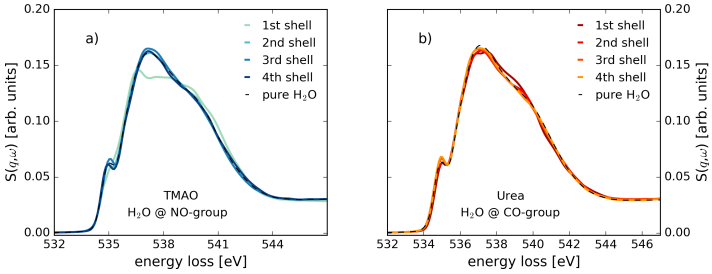

Fig. 3 a) Oxygen K-edge spectra of water molecules hydrating the hydrophilic side of the TMAO molecule at different distances denoted as 1st shell, 2nd shell, 3rd shell, and 4th shell in comparison to the calculated spectrum of pure water. b) Same as in a) but for water molecules hydrating the CO-goup of urea.

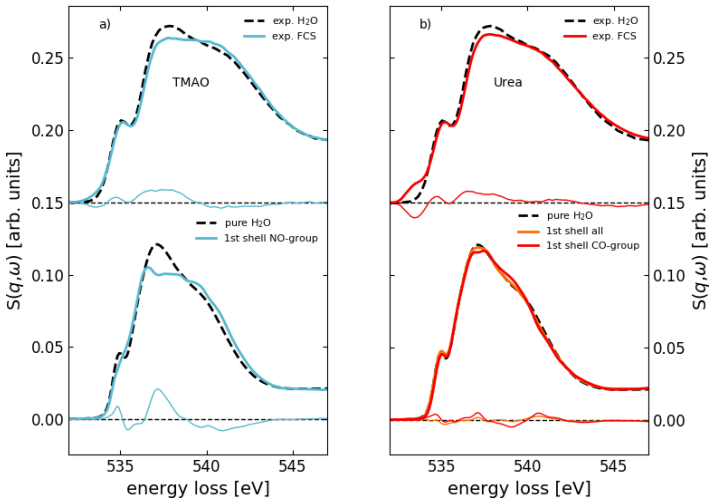

Fig. 4 Measured spectra of water and the free component spectra (FCS) extracted from experimental O K-edge spectra of concentration series of aqueous TMAO (a) and urea solutions (b) (top) compared to the calculated spectrum of pure water (dashed black lines) and the respective spectra from the first hydration shell of the NO-group in TMAO (a) and the CO-group in urea (b) (bottom). The similarity between the experimental FCS and the calculated spectra of the first shell are startling.

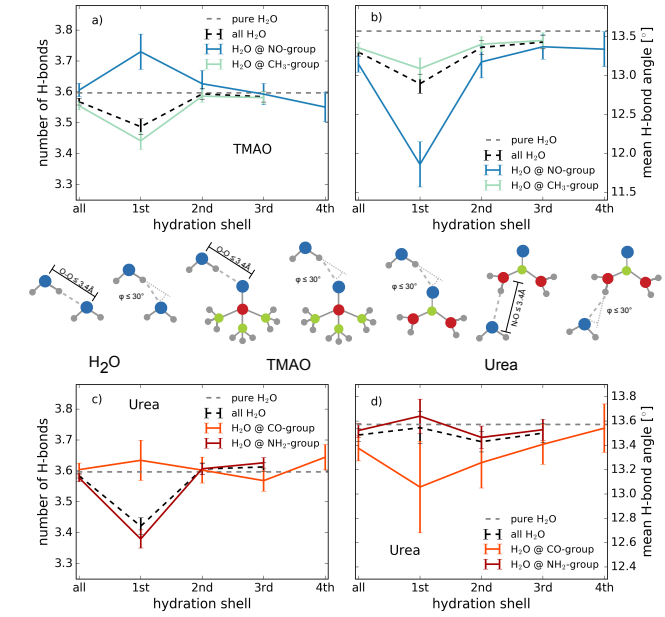

Fig. 5 Summary of selected structural parameters calculated for the hydration water molecules. a) Total number hydrogen bonds formed (both donated and accepted) for the different solvation shells in the TMAO solution. b) The mean hydrogen bond angle for the different solvation shells in the TMAO solution. c) Total number hydrogen bonds formed (both donated and accepted) for the different solvation shells in the urea solution. d) The mean hydrogen bond angle for the different solvation shells in the urea solution. Errorbars represent the standard deviation of the respective mean. Illustration of the geometric criteria for the hydrogen bond between two water molecules, between a water and a TMAO molecule, and between a water and an urea molecule are depicted in the middle.

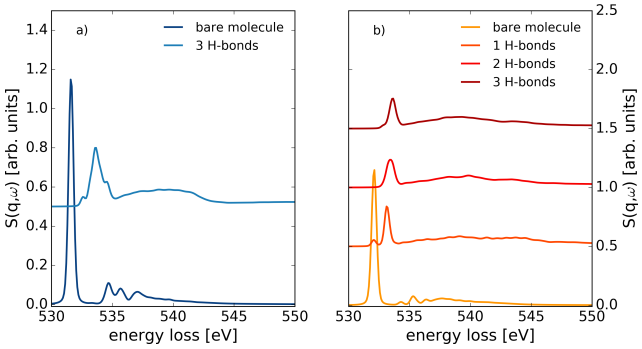

Fig. 6 a) Oxygen K-edge spectra of the oxygen atom of TMAO for the bare and hydrated molecule. b) K-edge spectra of the bare urea molecule and differently hydrated molecule from the trajectory.

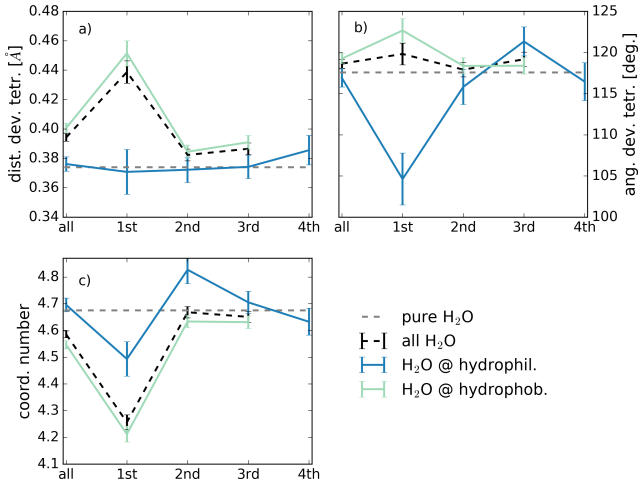

Fig. 7 a) Deviation from tetrahedrality in terms of distance. b) Deviation from perfect tetrahedrality in terms of angle. c) Coordination number of water molecules around the TMAO molecule in comparison with neat water (solid black line).

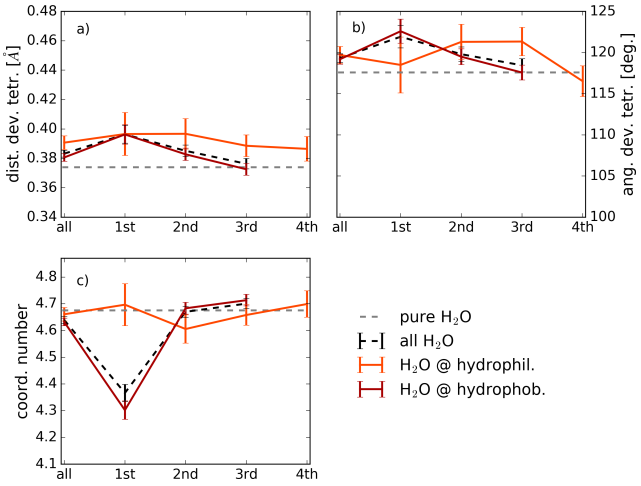

Fig. 8 a) Deviation from tetrahedrality in terms of distance. b) Deviation from perfect tetrahedrality in terms of angle. c) Coordination number of water molecules around the urea molecule in comparison with neat water (solid black line).

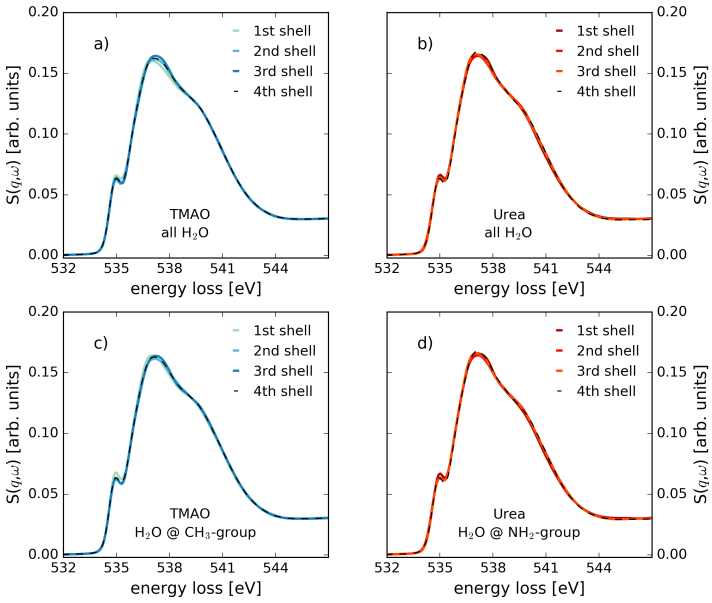

Fig. 9 a) Oxygen K-edge spectra of water molecules hydrating the TMAO molecule at different distances denoted as 1st shell, 2nd shell, and 3rd shell in comparison to the spectrum of pure water. Here, the set union of water molecules hydrating the hydrophilic and hydrophobic sides are shown. b) Same as in a) but for water molecules hydrating the urea molecule. c) Oxygen K-edge spectra of water molecules hydrating the hydrophobic side of the TMAO molecule at different distances denoted as 1st shell, 2nd shell, and 3rd shell in comparison with the spectrum of pure water. d) Oxygen K-edge spectra of water molecules hydrating the NH_2-goups of urea.

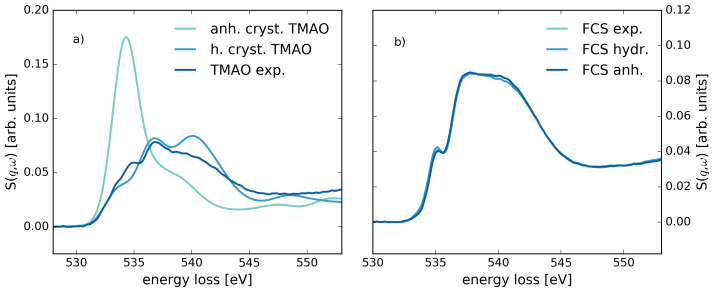

Fig. 10 a) Simulated oxygen K-edge spectra based on both hydrous and anhydrous TMAO crystal structures in direct comparison with the spectra measured from the TMAO polycrystalline reference sample. b) The different FCSs resulting from the use of the spectra shown in part a) for different non-negative matrix factorizations.